

Nanocarbon-assisted Carbon-nanotube-based Composite Electrodes for Improved Laccase Bio-electrocatalysis

Masato Tominaga,^{1*} Takuya Takatori,¹ Makoto Togami,² and Masayuki Tsushida³

¹Graduate School of Science and Engineering, Saga University,
1 Honjomachi, Saga 840-8502, Japan

²Graduate School of Science and Technology, Kumamoto University,
2-39-1 Kurokami, Kumamoto 860-8555, Japan

³Faculty of Engineering, Kumamoto University,
2-39-1 Kurokami, Kumamoto 860-8555, Japan

(Received March 27, 2023; accepted October 2, 2023)

Keywords: carbon nanotube, nanocarbon, laccase, electrocatalysis, oxygen reduction

Wearable devices have rapidly developed in recent years. The practical applications of wearable devices utilize secondary batteries such as lithium-ion batteries. Biofuel cells are a promising next-generation power source for these devices because they can be operated under mild conditions. Nanocarbons are essential materials owing to their excellent electrical conductivity and high surface area. However, nanocarbons easily aggregate, which results in an electrochemical active surface area significantly smaller than their theoretical individual surface area. Although carbon nanotubes (CNTs) have high electrical conductivity owing to their network structure and large specific surface area, it is well known that CNTs form bundled structures by aggregation. In this study, to completely exploit the properties of CNTs, a modified electrode was fabricated using a nanocarbon composite material with CNTs as the base material. Laccase bio-electrocatalysis tests were conducted, and the results clearly demonstrated the composite effect of CNTs with different nanocarbon morphologies, such as Ketjen black.

1. Introduction

Wearable devices for health maintenance have attracted considerable attention in recent years. Currently, it is possible to continuously measure blood oxygen concentration, obtain an electrocardiogram, and determine body temperature using a smart watch. However, the power sources for these measurements are secondary batteries such as lithium-ion batteries. Biofuel cells that use independently driven enzyme catalysis are expected to be the next-generation power sources for these wearable devices.⁽¹⁾ A biofuel cell is particularly suitable for combining with a wearable biosensor, which is a concept of enzymatic biofuel-cell-powered biosensors. This concept was easily achieved by Wang's group using screen-printing technology.⁽²⁾ Currently, many wearable biosensor types have been reported, such as the glucose biosensor,^(3,4) glutathione sensor,⁽⁵⁾ and diaper sensor.⁽⁶⁾ Such enzymatic biofuel-cell-powered biosensor

*Corresponding author: e-mail: masato@cc.saga-u.ac.jp
<https://doi.org/10.18494/SAM4407>

systems can be made from an anode and a cathode. Multicopper enzymes (MCEs) such as laccase, bilirubin oxidase, copper efflux oxidase, and ascorbate oxidase are powerful cathodes in enzymatic biofuel cells owing to their ability to reduce oxygen at a high potential without a mediator.^(7–14) Moreover, the MCE-catalyzed reaction can be achieved under mild conditions. The effective utilization of nanocarbons, which have excellent electrical conductivity and high surface area, is crucial for the realization of wearable biofuel cells.^(15–18) However, tailoring nanocarbons for application in electrodes is problematic because nanocarbons tend to agglomerate, and thus their theoretical surface area cannot be achieved. Carbon nanotubes (CNTs) are promising electrode materials for biofuel cells because of their high electrical conductivity, which originates from their network structure and large specific surface area.^(16,18–20) In contrast, it is very difficult to completely utilize the properties of CNTs to prepare electrodes because CNTs are significantly agglomerated compared with other nanocarbons. Therefore, in this study, we aim to completely exploit the properties of CNTs by fabricating electrodes using composites composed of nanocarbons with different morphologies and CNTs for application in laccase bio-electrocatalysis. The obtained results show that laccase bio-electrocatalysis clearly demonstrates the composite effect of CNTs with different nanocarbon morphologies, such as Ketjen black. Additionally, surface modification, which optimizes the molecular orientation of laccase adsorbed on the electrode, is demonstrated to be effective for nanocarbon composites with different surface properties.

2. Materials and Methods

2.1 Materials

Fungal laccase (Lac) from *Trametes sp.* (EC1.10.3.2) was obtained from Amano Enzyme (Nagoya, Japan) and purified as previously reported.^(21,22) All other chemical reagents were of analytical grade and were used as received without further purification. Single-walled carbon nanotubes (SWCNTs, diameter: 3–5 nm), OSAB (diameter: 10–30 nm), HS100 (diameter: 40–100 nm), H25 (size: 10–30 μm , thickness: *ca.* 10 nm), Ketjen black EC600JD (KB, diameter: 20–50 nm), and carbon black (CB, diameter: 1–5 μm) were used as nanocarbon materials. SG101 SWCNTs were provided by Zeon Co., Ltd. (Tokyo, Japan). OSAB and HS100 were provided by Denka Black Co., Ltd. (Tokyo, Japan). Plate-shaped pyrolytic graphite H25 was obtained from XG Science (Michigan, USA). KB and CB were purchased from Lion Specialty Chemicals Co., Ltd. (Tokyo, Japan) and Sigma–Aldrich (St. Louis, MO, USA), respectively. Panasonic graphite PGX 05 (Matsushita Electric Co., Japan) was used as the highly oriented pyrolytic graphite (HOPG). A glassy carbon (GC) disk electrode (outer diameter: 6 mm, inner diameter: 3 mm) was purchased from BAS Inc. (Tokyo, Japan). Sodium cholate (SC) was obtained from Wako Pure Chemical Industries (Osaka, Japan). All solutions were prepared using deionized water (resistivity > 18.2 M cm) obtained from a Milli-Q water purification system (Millipore, Billerica, MA, USA).

2.2 Electrode preparation and enzyme modification

The GC electrode was used as the support material for the nanocarbon modification process, which was performed as follows: The GC electrode was polished using a 0.05 μm alumina slurry, followed by sonication in ethanol and deionized water. A dispersed nanocarbon aqueous solution (5 mL) was prepared by mixing 5 mg of SWCNTs, 5 mg of nanocarbon, and 15 mg of SC, followed by dispersion for 10 min using probe-type ultrasonication (Branson 5520 sonicator, Kanagawa, Japan). Subsequently, a 5 μL aliquot of the dispersed carbon solution, which is equivalent to 10 μg of total mixed carbon (5 μg of SWCNTs and 5 μg of nanocarbon), was cast onto the GC disk electrode surface. The modified GC electrode was then dried under vacuum (~ 0.06 MPa). The nanocarbon-modified GC electrode was immersed in a 0.2 wt% SC aqueous solution for 30 min prior to enzyme modification.^(21,22) The electrode was gently rinsed by immersion in a 0.1 M acetate buffer (pH 5.0) to remove excess SC on the electrode surface. Subsequently, the electrode was immersed in a 5.0 μM Lac solution for 30 min and finally gently rinsed by immersion in a 0.1 M acetate buffer.

2.3 Instrumentation

Cyclic voltammetry measurements were performed on an electrochemical analyzer (ALS, Model 660A) using a conventional three-electrode cell with a Ag|AgCl|saturated KCl electrode (+199 mV vs a normal hydrogen electrode, NHE) as the reference electrode and a platinum wire as the counter electrode. In this study, all the reported potentials correspond to Ag|AgCl|saturated KCl at 25 °C. A 0.1 M acetate buffer solution (pH 5.0) was purged with high-purity argon before the measurements. During the electrochemical measurements, the buffer solution was vigorously stirred using a magnetic stirrer (800 rpm) to obtain voltammograms with a steady-state sigmoidal shape (plateau current). The saturated oxygen concentration was analyzed to be 1.24 mM using an oxygen meter (FireSting GO2, PyroScience GmbH, Aachen, Germany). The cell temperature was controlled at 25 ± 2 °C using a thermostated incubator.

Scanning electron microscopy (SEM) imaging was performed using a JSM-7600F microscope (JEOL, Japan). Transmission electron microscopy (TEM) was performed using a Tecnai F-20 field-emission microscope (Philips Electron Optics, The Netherlands).

Raman spectroscopy measurements were performed using a Horiba (Jobin Yvon) LabRAM HR-800 instrument with 514 nm (2.41 eV) laser excitation. Wavenumber calibration was performed using the emission of silica slides at 520 cm^{-1} .

The Brunauer–Emmett–Teller (BET) specific surface areas of the samples were determined from the N_2 adsorption and desorption isotherms at 77 K using a Quantachrome NOVA2200e instrument. Prior to the measurements, the samples were heated to 300 K for 24 h under vacuum to clean the sample surface. The peak radius and mesopore volume were determined using the Barrett–Joyner–Halenda method.⁽²³⁾

3. Results and Discussion

3.1 SEM and Raman spectroscopic characterization

Figure 1 shows SEM images of the nanocarbon materials, which were categorized into three types: (1) 1D nanocarbons with a diameter of 3–5 nm such as SG101 SWCNTs [Fig. 1(a)], (2) spherical nanocarbons with an aggregated secondary structure such as OSAB, HS100, KB, and CB [Figs. 1(b)–1(e)], and (3) 2D nanocarbons with a thickness of approximately 10 nm (H25) [Fig. 1(f)]. Raman spectroscopy is also useful for characterizing sp^2 -hybridized structures in carbon materials and provides information on defects and crystalline structures.^(24,25) Figure 2 shows the Raman spectra of the nanocarbons. All the nanocarbons exhibited characteristic peaks at approximately 1340 and 1570 cm^{-1} . The 1570 cm^{-1} peak was assigned to the G-band, which is the doubly degenerate phonon Raman-active mode for sp^2 -hybridized carbon networks. The D-band peak at 1340 cm^{-1} was attributable to the localization of regions where the lattice structure is imperfect, mostly at the edges and defects of sp^2 -hybridized carbon structures. SWCNTs [Fig. 2(a)] and H25 [Fig. 2(f)] exhibited a highly shared G-band peak and a weak D-band peak, which were similar to those observed in the Raman spectrum of the basal plane of HOPG [Fig. 2(g)]. In contrast, OSAB, KB, HS100, and CB [Figs. 2(b), 2(c), and 2(e)] showed a high D-band intensity, indicating that these nanocarbons are typical sp^3 -hybridized graphite-like structures with numerous structural defects at their surfaces. The intensity ratios of the G-band and D-band peaks are summarized in Table 1.

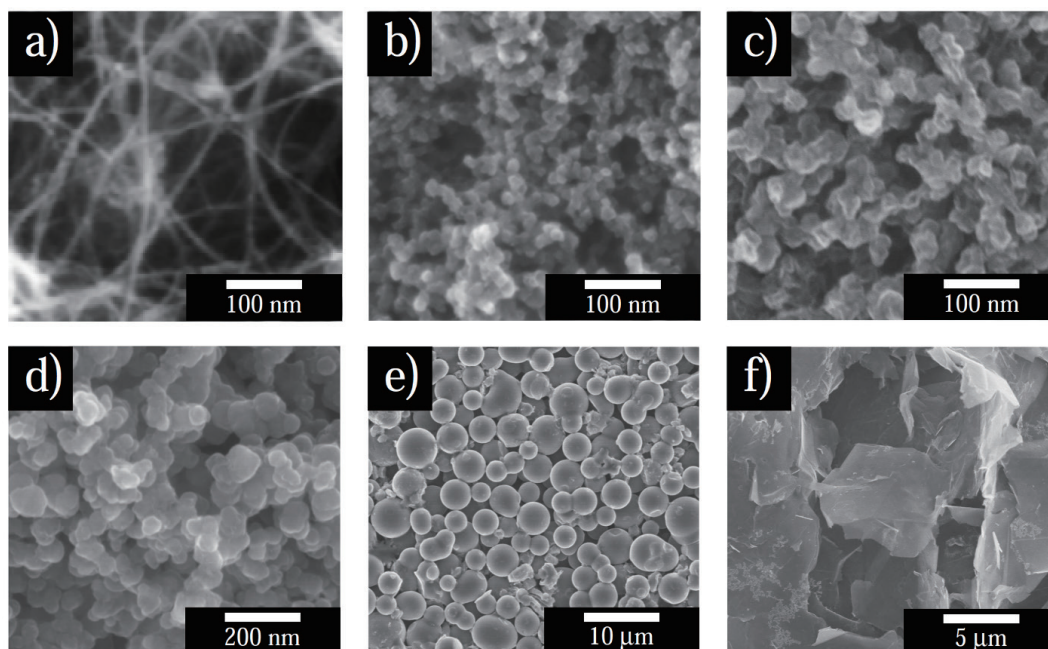


Fig. 1. SEM images of (a) SWCNT, (b) OSAB, (c) KB, (d) HS100, (e) CB, and (f) H25.

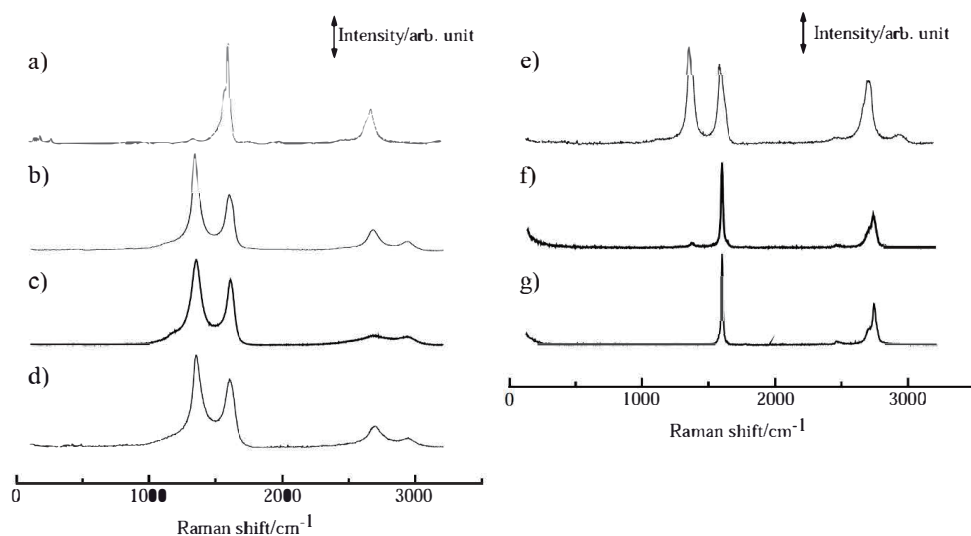


Fig. 2. Raman spectra of (a) SWCNT, (b) OSAB, (c) KB, (d) HS100, (e) CB, (f) H25, and (g) HOPG.

Table 1
Intensity ratio of G-band (I_G) to D-band (I_D).

Carbon	I_G/I_D
SWCNT	27
OSAB	0.6
KB	0.8
HS100	0.7
CB	0.8
H25	25
HOPG	124

3.2 Laccase bio-electrocatalysis

Figure 3 shows the catalytic oxygen reduction current based on the direct electron transfer reaction of laccase and each nanocarbon-modified electrode surface. A catalytic oxygen reduction current was observed from approximately 0.68 V, which is similar to the potential reported previously.^(21,22) This bio-electrocatalytic current strongly depended on the type of nanocarbon mixed with the SWCNTs. Compared with the SWCNT-modified electrode, the electrodes modified with the KB-SWCNT [Fig. 3(c)] and OSAB-SWCNT [Fig. 3(b)] composites exhibited almost 2 and 1.5 times higher current values, respectively. On the basis of these results, the Lac bio-electrocatalytic performance characteristics of the KB-SWCNT- and OSAB-SWCNT-modified electrodes were investigated. However, the KB-SWCNT and OSAB-SWCNT composites easily peeled off the GC electrode surface and were observed in the buffer solution. This indicates that a certain degree of SWCNT aggregation is required to fabricate a stable

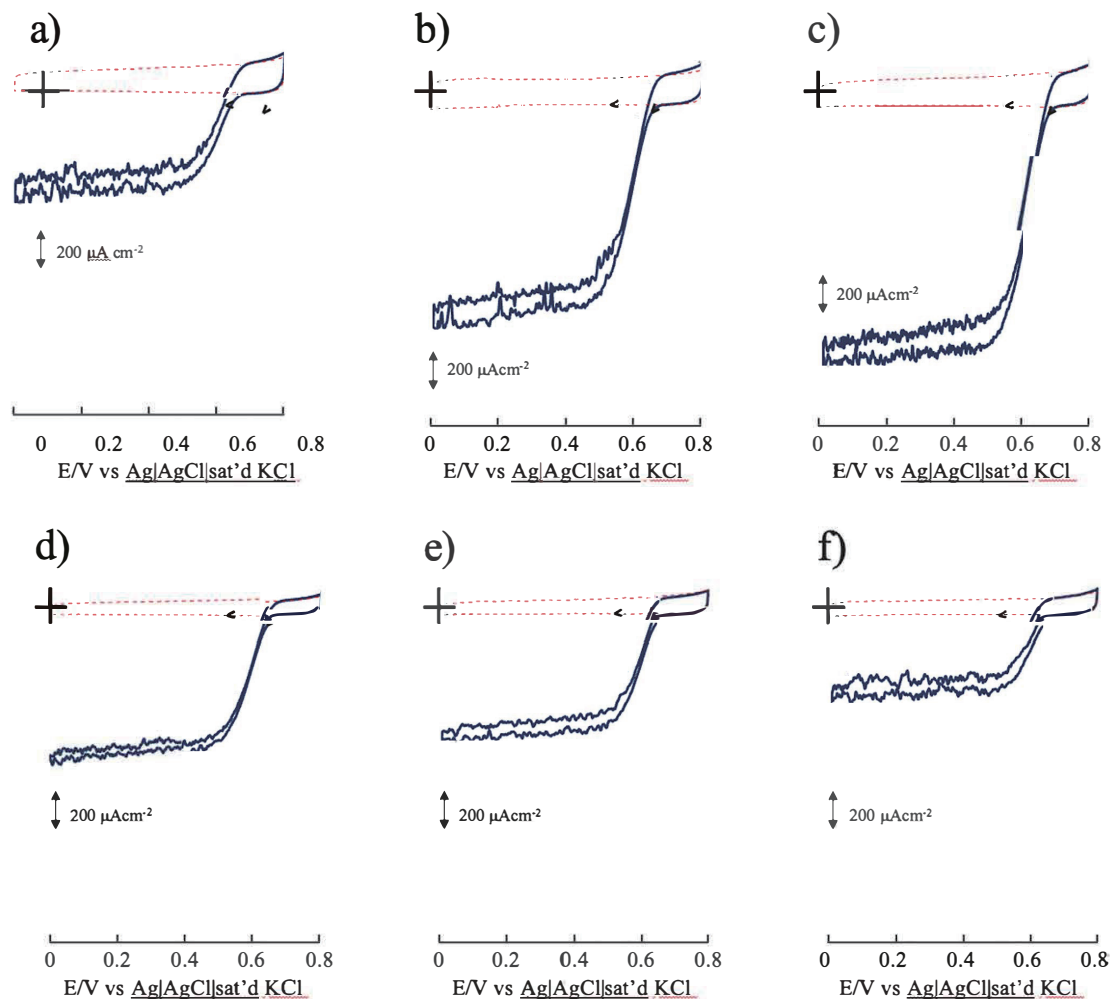


Fig. 3. Cyclic voltammograms of (a) SWCNT, (b) OSAB-SWCNT, (c) KB-SWCNT, (d) HS100-SWCNT, (e) CB-SWCNT, and (f) H25-SWCNT modified with Lac in 0.1 M acetate buffer solution (pH 5.0) in the presence of O_2 .

modified electrode. Electrodes modified with CB-SWCNT [Fig. 3(e)] and HS100-SWCNT [Fig. 3(d)] composites exhibited almost the same catalytic current magnitude as the SWCNT-modified electrode. However, the catalytic current of the HS25-SWCNT-modified electrode [Fig. 3(f)] was slightly lower than that of the SWCNT-modified electrode [Fig. 3(a)]. Upon oxygen reduction, an onset potential of approximately 0.68 V was observed, which was independent of the type of nanocarbon used in the composite. Similarly, the half-wave potential, which indicates the potential at half the oxygen catalytic current, did not depend on the type of nanocarbon used; the half-wave potential was determined to be 0.58–0.59 V. These findings strongly indicate that the electron transfer kinetics between Lac and the electrode are similar for the different nanocarbon-SWCNT-modified electrodes. Thus, it is reasonable to suggest that the difference in catalytic oxygen reduction current between the different nanocarbons is attributable to the number of Lac molecules adsorbed on the nanocarbon surface.

3.3 Specific surface area dependence of catalytic current

Table 2 (left column) shows the BET surface area (S_{BET}) values determined by N_2 adsorption and desorption at 77 K. Generally, the trend in the catalytic current magnitude is related to the measured surface area. That is, the KB-SWCNT composite exhibited the highest catalytic current intensity and the highest surface area among the different nanocarbon-SWCNT composites used in this study. In contrast, the surface area of H25 was approximately three times higher than that of the SWCNTs, although the catalytic current intensities were similar. The surface area was analyzed more carefully because it is dependent on the size of the adsorbed molecules. The Lac molecule (approximately 7 nm in diameter) is significantly larger than the N_2 molecule, indicating that adsorption is limited for the Lac molecule compared with the N_2 molecule.⁽²⁶⁾ Table 2 (middle and right columns) shows the surface area ($S_{10\text{nm}}$) results, which exclude pore sizes smaller than 10 nm, and the $S_{10\text{nm}}/S_{\text{BET}}$ ratio of $S_{10\text{nm}}$ relative to the total BET surface area S_{BET} . For the SWCNTs, the $S_{10\text{nm}}/S_{\text{BET}}$ ratio was 13%, which is reasonable because it is well known that CNTs, especially SWCNTs, easily form bundles.⁽²⁷⁾ The bundled SWCNTs provide approximately 10% of the S_{BET} for effective Lac adsorption. Additionally, the $S_{10\text{nm}}/S_{\text{BET}}$ ratio (13%) of the H25-SWCNTs was similar to that of the SWCNTs. Figure 4 shows a plot of the catalytic current as a function of S_{BET} for the nanocarbon-SWCNT composites. The catalytic current increased linearly with $S_{10\text{nm}}$, except for the H25-SWCNT composite. This behavior is interesting because the nanocarbon surface conditions show large differences in the defects and crystalline structures, as shown in Fig. 2. Generally, it is recognized that enzyme electrocatalysis strongly depends on the electrode surface conditions, such as hydrophobicity/hydrophilicity and negative/positive charges. In this study, the sodium collate of a biosurfactant was used as the surface modifier.^(11,22) Therefore, it was concluded that, although the surface was not optimal for the electrode reaction with Lac, surface modification may provide optimal conditions for the Lac electrode reaction.

Figure 5 shows TEM images of the SWCNTs and KB-SWCNTs. The aggregated and bundled SWCNT structures were observed only in the SWCNTs [Fig. 5(a)]. In contrast, in the KB-SWCNTs [Fig. 5(b)], the aggregation and bundling of the SWCNTs were inhibited well by KB, which clearly demonstrates why the KB-SWCNT composite exhibited the highest $S_{10\text{nm}}$ and the highest catalytic current among the different nanocarbon-SWCNT composites used in this study. Also, the OSAB-SWCNT composite was significantly effective for increasing the Lac bioelectrocatalytic performance and $S_{10\text{nm}}$. These results suggest that, taking into account the fact

Table 2
Surface areas of nanocarbon-SWCNT composites.

Carbon	Surface area (S_{BET}) / $\text{m}^2 \text{g}^{-1}$	Surface area ($\sim 10 \text{ nm}$) ($S_{10\text{nm}}$) / $\text{m}^2 \text{g}^{-1}$	$S_{10\text{nm}} / S_{\text{BET}} \%$
SWCNT	4.8	0.64	13
OSAB-SWCNT	36	21	58
KB-SWCNT	51	38	75
HS100-SWCNT	18	7.7	43
CB-SWCNT	7.8	5.5	71
H25-SWCNT	16	2.0	13

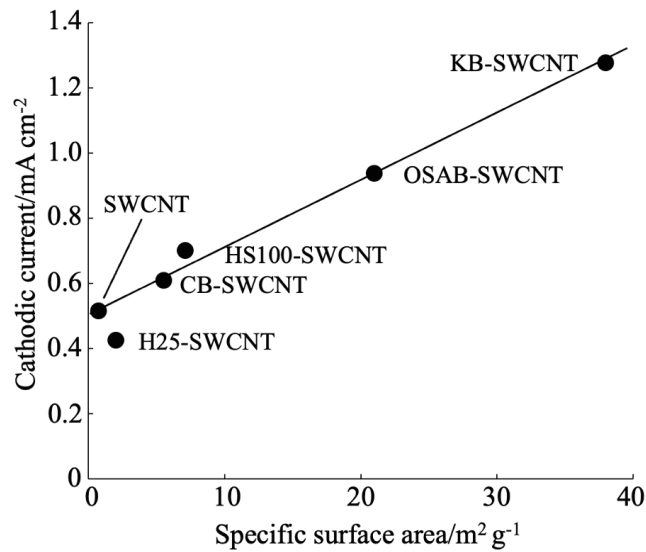


Fig. 4. Catalytic oxygen reduction current as a function of $S_{10\text{nm}}$ (specific surface area = ~ 10 nm).

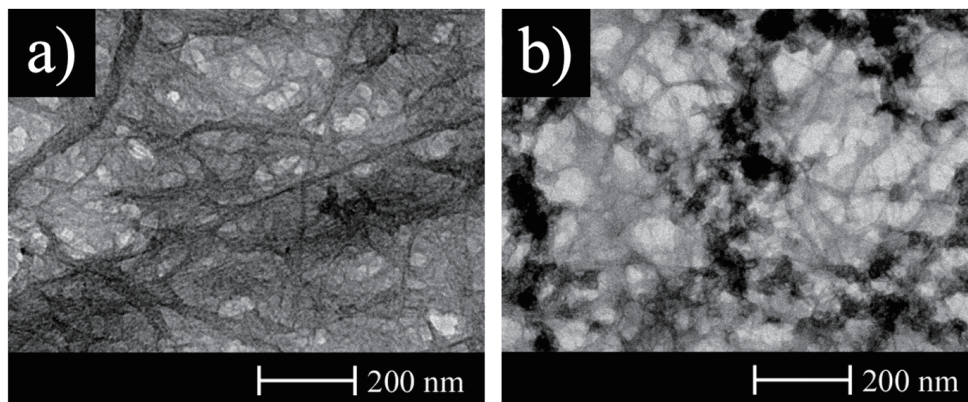


Fig. 5. TEM images of (a) SWCNTs and (b) KB-SWCNTs.

that the KB and OSAB sizes are less than those of the other nanocarbons, the inhibition effect on the aggregation and bundling of SWCNTs would strongly depend on the size of the nanocarbons.

4. Conclusions

The composite effect of nanocarbons with SWCNTs on Lac bio-electrocatalysis was clarified using a sodium-collate-modified carbon electrode. In particular, KB was considered effective as a composite nanocarbon with SWCNTs. KB inhibited SWCNT aggregation and bundling, resulting in an amplified catalytic oxygen reduction current compared with the catalytic current obtained using only SWCNTs. Surface modification with sodium collate provides suitable

electrode surface conditions for Lac bio-electrocatalysis. Thus, although the surfaces of the nanocarbon crystal structures were not the same, the magnitude of Lac bio-electrocatalysis strongly depended only on the specific surface area. The results of this research provide useful information for design and adjustment methods in cathode development for enzymatic biofuel cell-powered biosensors.

Acknowledgments

The authors acknowledge Denka Co., Ltd. for kindly providing OSAB and HS-100. The authors also thank Zeon Co., Ltd. for kindly providing SG101 SWCNTs.

References

- 1 T. Takamatsu, Y. Sijie, F. Shujie, L. Xiaohan, and T. Miyake: *Adv. Funct. Mater.* **30** (2019) 1906225. <https://doi.org/10.1002/adfm.201906225>
- 2 I. Jeerapan, J. R. Sempionatto, A. Pavinatto, J. M. You, and J. Wang: *J. Mater. Chem. A* **4** (2016) 18342. <https://doi.org/10.1039/C6TA08358G>
- 3 Y. Zhang, S. Hao, X. Sun, H. Zhang, Q. Ma, J. Zhai, and S. Dong: *Electroanalysis* **34** (2022) 1953. <https://doi.org/10.1002/elan.202100417>
- 4 A. Sanati, Y. Esmacili, E. Bidram, L. Shariati, M. Rafienia, S. Mahshid, and O. Parlak: *Appl. Mater. Today* **26** (2022) 101350. <https://doi.org/10.1016/j.apmt.2021.101350>
- 5 B. G. Roy, J. L. Rutherford, A. E. Weaver, K. Beaver, and M. Rasmussen: *Biosensors* **10** (2020) 114. <https://doi.org/10.3390/bios10090114>
- 6 I. Shitanda, Y. Fujimura, T. Takarada, R. Suzuki, T. Aikawa, M. Itagaki, and S. Tsujimura: *ACS Sens.* **6** (2021) 3409. <https://doi.org/10.1021/acssensors.1c01266>
- 7 N. Mano and A. de Poulpiquet: *Chem. Rev.* **118** (2018) 2392. <https://doi.org/10.1021/acs.chemrev.7b00220>
- 8 M. T. Meredith, M. Minson, D. Hickey, K. Artyushkova, D. T. Glatzhofer, and S. D. Minter: *ACS Catal.* **1** (2011) 1683. <https://doi.org/10.1021/cs200475q>
- 9 S. Shleev, J. Tkac, A. Christenson, T. Ruzgas, A. I. Yaropolov, J. W. Whittaker, and L. Gorton: *Biosens. Bioelectron.* **20** (2005) 2517. <https://doi.org/10.1016/j.bios.2004.10.003>
- 10 S. Shleev, V. Andoralov, D. Pankratov, M. Falk, O. Aleksejeva, and Z. Blum: *Electroanalysis* **28** (2016) 2270. <https://doi.org/10.1002/elan.201600280>
- 11 J. A. Cracknell, K. A. Vincent, F. and A. Armstrong: *Chem. Rev.* **108** (2008) 2439. <https://doi.org/10.1021/cr0680639>
- 12 N. Loew, I. Shitanda, H. Goto, H. Watanabe, T. Mikawa, S. Tsujimura, and M. Itagaki: *Sci. Rep.* **12** (2022) 14649. <https://doi.org/10.1038/s41598-022-19052-4>
- 13 R. D. Milton and S. D. Minter: *Interface* **14** (2017) 20170253. <https://doi.org/10.1098/rsif.2017.0253>
- 14 S. Lorcher, P. Lopes, A. Kartashov, and E. E. Ferapontova: *ChemPhysChem* **14** (2013) 2112. <https://doi.org/10.1002/cphc.201300069>
- 15 J. Kim, I. Jeerapan, J. R. Sempionatto, A. Barfidokht, R. K. Mishra, A. S. Campbell, L. J. Hubble, and J. Wang: *Acc. Chem. Res.* **51** (2018) 2820. <https://doi.org/10.1021/acs.accounts.8b00451>
- 16 S. Ul Haque, M. Yasir, and S. Cosnier: *Biosens. Bioelectron.* **214** (2022) 114545. <https://doi.org/10.1016/j.bios.2022.114545>
- 17 A. Sanati, Y. Esmacili, E. Bidram, L. Shariati, M. Rafienia, S. Mahshid, and O. Parlak: *Appl. Mat. Today* **26** (2022) 101350. <https://doi.org/10.1016/j.apmt.2021.101350>
- 18 I. Shitanda, Y. Fujimura, T. Takarada, R. Suzuki, T. Aikawa, M. Itagaki, and S. Tsujimura: *ACS Sensor* **6** (2021) 3409. <https://doi.org/10.1021/acssensors.1c01266>
- 19 Y. Kamitaka, S. Tsujimura, N. Setoyama, T. Kajino, and K. Kano: *Phys. Chem. Chem. Phys.* **9** (2007) 1793. <https://doi.org/10.1039/B617650J>
- 20 M. Tominaga, K. Kuwahara, M. Tsushida, and K. Shida: *RSC Adv.* **10** (2020) 221200. <https://doi.org/10.1039/D0RA03476B>
- 21 M. Tominaga, M. Togami, M. Tsushida, and D. Kawai: *Anal. Chem.* **86** (2014) 5053. <https://doi.org/10.1021/ac500700h>

- 22 M. Tominaga, A. Sasaki, M. Tsushida, and M. Togami: *New. J. Chem.* **41** (2017) 231–236. <https://doi.org/10.1039/C6NJ02287A>
- 23 S. Brunauer, P.H. Emmett, and E. Teller: *J. Am. Chem. Soc.* **60** (1938) 309. <https://doi.org/10.1021/ja01269a023>
- 24 F. Tuinstra and J. L. Koenig: *J. Chem. Phys.* **53** (1970) 1126. <https://doi.org/10.1063/1.1674108>
- 25 F. Tuinstra and J. L. Koenig: *J. Compos. Mater.* **4** (1970) 492. <https://doi.org/10.1177/002199837000400405>
- 26 K. Pionetek, M. Antorini, and T. Choinowski: *J. Biol. Chem.* **277** (2002) 37663. <https://doi.org/10.1074/jbc.M204571200>
- 27 M. Tominaga, S. Sakamoto, H. Yamaguchi: *J. Phys. Chem.* **116** (2012) 9498. <https://doi.org/10.1021/jp2112473>